Physical properties of quasi-one-dimensional MgO and Fe_3O_4-based nanostructures

J. Mejía-López,[1] J. Mazo-Zuluaga,[2,*] S. López-Moreno,[3] F. Muñoz,[4] L. F. Duque,[5] and A. H. Romero[6]

[1]*Facultad de Física, Pontificia Universidad Católica de Chile, and CEDENNA, Santiago, Chile*

[2]*GICM and GES Groups, IF-FCEN, Universidad de Antioquia, Calle 70 Número 52-21, Medellín, Colombia*

[3]*Escuela Superior Ciudad Sahagún, Universidad Autónoma del Estado de Hidalgo, Carretera Ciudad Sahagún-Otumba s/n, 43990 Hidalgo, México*

[4]*Departamento de Física, Facultad de Ciencias, Universidad de Chile, and CEDENNA, Santiago, Chile*

[5]*Centro de Ciencias de la Computación, Instituto Tecnológico Metropolitano, Medellín, Colombia*

[6]*Physics Department, West Virginia University, Morgantown, West Virginia 26506-6315, USA*

(Received 10 February 2014; revised manuscript received 6 June 2014; published 11 July 2014)

We have studied the properties of several representative one-dimensional structures—MgO nanowires, Fe_3O_4 hollow nanotubes, Fe_3O_4 nanowires, and MgO/Fe_3O_4 core/shell nanotubes—by means of first-principles-based calculations. Each of these nanostructures reveals different electronic properties with novel electronic states due to the large surface/interface of the nanocylinders. Electronic states of the Fe_3O_4 nanowire are localized around small clusters of atoms, and its bands appear with almost no energy dispersion. Localization is not a direct consequence of structural disorder; instead, it seems to be induced by an enhanced charge transfer due to the undercoordination on the surface. The combined effect of the MgO/Fe_3O_4 nanostructure shows that the MgO is well coated and even bulk-like states can be observed. However, the magnetite suffers important atomic reconstructions losing symmetries and increasing its atomic-like behavior. Effects of axial deformations on the properties and the relation of the results to potential technological applications are discussed.

DOI: 10.1103/PhysRevB.90.035411 PACS number(s): 73.22.−f, 71.15.Mb, 61.46.Bc, 75.50.Gg

I. INTRODUCTION

Since early 1980s, with the discovery of carbon-based nanostructures such as buckyballs, carbon nanotubes, and fullerenes, the fabrication of hollow nanostructures not only has attracted great attention but also has employed an increasingly wide variety of materials. Additionally, several synthesis mechanisms have been studied and continuously developed, with the aim to obtain control over size distribution and morphological features of different kinds of structures useful in nanoscience and nanotechnology [1].

In very recent years, the interest in complex inorganic hollow nanostructures has increased tremendously due to their peculiar properties and amazing advantages for applications in several fields such as nanofluidics, nanoscale electronics or spintronics, high-density magnetic data storage, and gas sensor devices. In particular, nanowires and nanotubes made of transition metals and their respective oxides are offering an active research field from both fundamental and experimental viewpoints. These low-dimensional structures offer the medium for one-dimensional transport at the nanometric scale that will be used in near-future electronic devices. Along with the increasing interest in these advanced structures, there is a need for theoretical studies to better understand phenomena at this small size scale and their dimensionality dependence.

On the other hand, magnetite (Fe_3O_4), due to its high Curie temperature (around 859 K), half-metallic properties, large spin polarization at room temperature, and magnetic properties tunable by size, shape, and dimension, became one of the most studied magnetic nanomaterials. Due to its complex structure and unique electronic, magnetic, and biocompatible properties, magnetite offers a wide range of uses including technological applications such as spintronics [2], new ferrofluids [3], magnetoelectronic devices [4], nanoelectromechanical systems [5,6], and gas sensors [7], and biomedical and biotechnological uses such as drug targeting delivery [8], thermal treatments and contrast enhancement in magnetic resonance imaging [9], catalysis [10] and magnetic separation of cancer cells [9], biosensors [11], and functionalized nanostructures [12–14], among others [15–17].

Regarding the fabrication of iron-oxide-based one-dimensional nanostructures, some studies on fabrication and characterization of nanowires [18,19], nanobelts [18,19], nanotubes [20,21], and nanotube arrays [22,23] have been recently reported. Additionally, 1D core/shell nanostructures have exhibited exciting physical properties. To illustrate, it has been found that, due to their nearly full spin polarization at room temperature, 1D magnetite nanostructures are good candidates for giant magnetoresistance and spin valve devices [7,20,24–26]. Also, they can be used for magnetic and electromagnetic wave absorption applications in order to fight expanded electromagnetic interference problems [27,28]. Likewise, the Kirkendall-based fabrication route and the Wagner counterdiffusion mechanism have been employed to built iron oxide nanotubes, nanowires, and nanorods [1,29]. Moreover, significant achievements have been made in developing a nonequilibrium synthesis technique to produce a wide variety of transition metal oxide core/shell nanowires, specifically on MgO/Fe_3O_4 core/shell nanotubes, aiming to transport applications [30] and magnetoresistance studies for nanoelectronics/spintronics uses [24,25].

The applicability of new properties of quasi-1D nanostructures to current technology portends a growing field of research. In particular, Cu and Cu oxide nanowires and nanotubes arrays could be used for enhancing the capacity retention of rechargeable batteries [31]. Within the biomedical

*Corresponding author: johanmazo@gmail.com

field, multiwalled carbon nanotubes have been considered in the controlled delivery of drugs [32]. A special nanosyringe was proposed, with the potential to deliver drugs in a controlled way, obtaining selective cell destruction and reduced toxicity, in contrast to the nondiscriminative cell destruction of the conventional free drug approach [33]. These authors also pointed out the significant need for more basic theoretical studies on tubular nanostructures to better understand their properties and facilitate soon practical/therapeutic implementation. Concerning transport properties, in 1D metal oxide structures, the control of electrons and holes has been explored for applications to nanodevices. Recently, an interesting effect has been observed regarding the transition between n- (electrons) and p-type (holes) transport occurring in metal oxides. This transition can be achieved by means of an annealing process that generates a change of the dominant carriers (electrons or holes) at the sample surface. This n-p transition has been observed in SnO_2, MoO_3, In_2O_3 [34], and α-Fe_2O_3 thin films [35]. The inverse transition, namely p to n type, was also recently reported to take place in α-Fe_2O_3 nanowires annealed in a reductive atmosphere, which gave impulse to a structural transition into magnetite nanowire, and an n-type nature of the transport properties was observed (i.e., a p- to n-type transition of the carrier scheme) [36,37].

On the other hand, although Moore's law remains valid in the microelectronics field, it is expected that, a certain size onwards, it will be no longer valid. In fact, beyond the difficult issues regarding heat dissipation, scaling down devices to lengths in the nanometer scale—coming from microelectronics towards nanoelectronics—has fundamental implications related with the effect of confinement and disorder on the behavior of the electronic and magnetic properties of the nanometric materials that compose these devices. Then, the relevance is clear of studying, from the basic point of view, the compounds of potential interest for the application fields already mentioned.

Despite the increasing importance of all these features related to one-dimensional nanostructures, to our knowledge, there are no first-principles studies of 1D magnetite-based structures published yet. Therefore, in this study, we employ first-principles methods to analyze the properties of several one-dimensional structures: a MgO nanowire, a Fe_3O_4 hollow nanotube, a Fe_3O_4 nanowire, and a MgO/Fe_3O_4 core/shell nanotube. Thus, this paper is designed to provide valuable information on the structural, electronic, and magnetic properties of the mentioned 1D nanostructures, as well as on the effect of contraction and stress forces on their properties aiming at both basic scientific interest and potential technological applications.

II. THEORETICAL METHODS

In spite of the mentioned studies on construction, characterization, and applications of new properties of tubular structures, it is worth pointing out that their basic physics remains to be explored. Therefore, we focus our interest on the following systems: (a) MgO nanowire (MgONW), (b) magnetite nanowire (MNW), (c) hollow magnetite nanotube (MNT), and (d) MgO/Fe_3O_4 core/shell nanotube (CSNT); each of them represents a different case of such 1D systems. The external average diameter for the nanostructures that contain magnetite (MNW, MNT, and CSNT) was 1.4 nm, while for the MgONW was 0.6 nm. MNT has an internal diameter for the hole of around 0.6 nm as well. Thus, quasi-1D samples of the studied structures were growth along the c axis and simulated by periodic cells separated by a sufficiently large vacuum slab in order to avoid spurious intertube interactions. Hence, our simulated system can be considered as a periodic array of isolated cylinders. For completeness and comparison purposes, bulk Fe_3O_4 and bulk MgO systems are also considered and taken as reference materials. The $Fd\bar{3}m$ crystalline structure was selected to built magnetite nanostructures, while the MgO systems were simulated by considering its rocksalt structure with space group $Fm\bar{3}m$. The choice of the MgO compound is based on the fact that this oxide has been used as template for obtaining core/shell nanotube samples [24,25,30] due to the almost perfect match between the magnetite and the MgO [38] (the mismatch is around 0.4%).

We perform a density functional theory (DFT) [39,40] study using the VASP package [41,42] with projector augmented wave (PAW) pseudopotentials [43,44]. The exchange and correlation energy was described within the generalized gradient approximation (GGA) in the Perdew-Burke-Ernzerhof (PBE) prescription [45]. The GGA + U approach was used to account for strong correlation between the electrons in the Fe d shell [46], where a U_{eff} ($= U - J^{\text{H}}$) is considered. We have used $U = 4.5$ eV and $J^{\text{H}} = 0.89$ eV for Fe atoms [47–50]. These values have been already reported in previous electronic structure studies for magnetite-based systems, where good agreement of a large diversity of properties has been reported [17,51]. Besides, even though we have used the bulk values for the Coulomb repulsion parameters (J, U), we did find a weak dependence of the atomic charge and the atomic magnetic moment for values of U_{eff} ranging from 2.5 to 6.5. This indicates that the properties are not very sensitive to the choice of U_{eff} but its presence is important to describe correctly the electronic and magnetic properties of the systems.

The Birch-Murnaghan equation of state [52] was employed to fit the total energy to obtain the equilibrium parameters for the bulk magnetite and MgO samples. For all structures considered here we perform a careful ionic relaxation until forces were negligible (less than 0.01 eV/Å). We use a kinetic energy cutoff of 520 eV for the expansion of the plane waves, which is high enough to ensure the completeness of the basis.

For integrations in the Brillouin zone, the k-point mesh was set to $1\times1\times3$ for MNW, MNT, and CSNT structures; while for magnetite bulk, MgO bulk, and MgONW we used $6\times6\times6$, $12\times12\times12$, and $1\times1\times12$ k-point grids, respectively. For self-consistence calculations, with the aim to show details of the energy spectrum, a denser $22 \times 22 \times 22$ k grid has been employed in the MgO bulk case, whereas calculations of the DOS for the bulk magnetite have been carried out on a $12 \times 12 \times 12$ k-space grid, and $1 \times 1 \times 40$ k-space grids were used for the other 1D structures.

Wigner-Seitz radii $r_{\text{WS}} = 1.302$ and $r_{\text{WS}} = 0.82$ Å were used for Fe and O, respectively. The charge of each atom was estimated by using the Bader method, where a fair partition of the electronic charge is performed by including only the valence electrons. Implementation details can be found in Ref. [53]. The magnetic moment distribution was computed

by integrating the electronic density within the Wigner-Seitz radius for each atom. The overall magnetizations per system were also determined.

To study the effect on the structural and energetic properties of the systems, cohesive energies E_b were also computed according to

$$E_b = \frac{E_{\text{tot}} - N_{\text{Fe}}E_{\text{Fe}} - N_{\text{O}}E_{\text{O}} - N_{\text{Mg}}E_{\text{Mg}}}{N_{\text{Fe}} + N_{\text{O}} + N_{\text{Mg}}}, \qquad (1)$$

where N_{Fe}, N_{O}, and N_{Mg} correspond to the number of Fe, O, and Mg atoms with energies in the isolated state E_{Fe}, E_{O}, and E_{Mg}, respectively. To have a full structural characterization of the nanostructures, histograms, which show how the atoms become spatially distributed in samples as well as the radial distribution function [RDF or $g(r)dr$], were also computed. The RDF function accounts for the number of neighbors surrounding every atom at a given distance between r and $r + dr$. Finally, the effects of strain and compression on the electronic and magnetic properties of the quasi-1D structures studied have also been considered.

III. RESULTS AND DISCUSSION

Figure 1 illustrates the structures of the systems studied after relaxation. For simulating magnetite we used the primitive cell with 14 atoms (2 formula units: f.u.), while for bulk MgO the system is composed of two atoms (1 f.u.). All quasi-1D samples were grown along the c axis with a length of 0.8448 nm (i.e., the length of the cell parameter for magnetite).

In Table I we show the ground-state lattice parameters and some electronic properties for $Fd\bar{3}m$ bulk magnetite and $Fm\bar{3}m$ bulk MgO structures, our reference materials, obtained in the present calculations. Experimental data and theoretical results are also listed for comparison. As can be observed, for both cases, results are in agreement with experimental data and several theoretical reports [54–64]. This last fact gives confidence on the calculation method and make us think that the above description captures all the relevant physics and is a good starting point to present the results for the proposed nanostructures. For reference and comparison of the structural characterization for 1D systems, Table II reports mean equilibrium distances for several types of nearest neighbor (nn) bonds in both bulk systems.

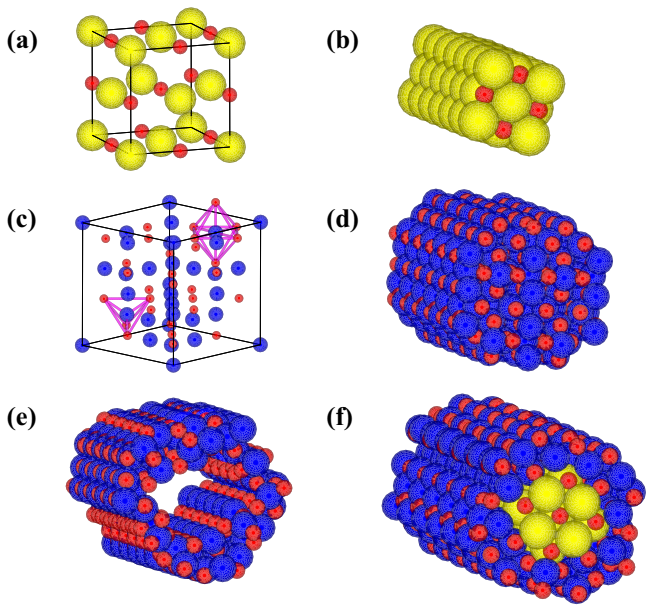

FIG. 1. (Color online) Schematic view of (a) the MgO unit cell, (b) the MgONW, (c) the magnetite unit cell, which illustrates explicitly a tetrahedral and an octahedral site, (d) the MNW, (e) the MNT, and (f) the CSNT. Small red spheres represent O atoms, while yellow spheres stand for Mg and blue ones for Fe atoms.

TABLE I. Ground-state lattice parameters and electronic properties for the bulk cubic Fe_3O_4 and bulk MgO structures. Lattice constants (a) are expressed in Å, cohesive energies per atom (E_b) and electronic gaps (Δ_g) are in eV, magnetic moments per f.u. (μ) are given in μ_B, and bulk modulus (B) are in GPa.

	This work	Literature	Experimental
Fe_3O_4			
a	8.448	8.446 [54,55]	8.394 [56,57]
E_b	−5.154		
Δ_g	0	0 [54,55]	0
μ	4.00	3.96 [54,55]	4.05 [58]
B	138.46		141–222 [59]
MgO			
a	4.238	4.234 [60]	4.211 [64]
E_b	−5.153		
Δ_g	4.6	4.5–5 [60,61]	7.8–8.2 [62]
μ	0	0 [63]	0
B	150	150.6 [63]	160.2 [64]

A. Structural analysis

Table III registers some results for the studied systems. The first aspect to highlight is that all systems are energetically stable structures. Bulk samples share the most stable values and very similar cohesive energies per atom, while among the quasi-1D nanostructures, CSNT obtains a configuration with favorable cohesive energy per atom as compared with MgONW and MNT (the two structures that compose the CSNT), and MNW is the most stable system.

Furthermore, since magnetite exhibits biocompatibility, it can be synthesized in one-dimensional shapes, and recalling one of the exciting proposals for technological applications to the nano-biomedical field, it is plausible to consider these

TABLE II. Equilibrium distances (in Å) for nn bonds in bulk Fe_3O_4 and bulk MgO.

Fe_3O_4		MgO	
type	nn distance	type	nn distance
Fe_A-O	1.90	Mg-O	2.12
Fe_B-O	2.08	Mg-Mg	3.00
Fe_A-Fe_A	3.66	O-O	3.00
Fe_A-Fe_B	3.51		
Fe_B-Fe_B	2.99		
O-O	2.88		

TABLE III. Some parameters for the different systems. N represents the number of atoms in the supercell used to simulate the sample. Cohesive energy per atom, E_b, and electronic band gap, Δ_g, are given in eV. Magnetic moments per f.u., μ, are given in μ_B. The size of the supercell parameter in z direction, Z, is given in Å.

Structure	N	E_b	μ	Z	Δ_g
Bulk MgO	2	−5.153	0	4.238	4.60
MgONW	18	−4.831	0	3.972	3.09
Bulk Fe_3O_4	14	−5.154	4.00	8.448	0.00
MNW	127	−4.997	5.32	8.394	0.48
MNT	106	−4.801	5.00	8.198	0.18
CSNT	134	−4.960	4.57	8.392	0.48

MNTs as a potential source and very promising material for the development of the nanosyringe proposed by Hilder and Hill [32,33].

The longitudinal lattice parameter indicates that a notable contraction along the axial (z) direction is obtained in the 1D structures as compared to the bulk systems. This result can be explained as a coordination reduction of most atoms sitting on the free surface, which induces larger electron transfer from neighboring atoms. To explore this, we have performed a Bader charge analysis, which shows, for example, that in the MgONW a partial charge transfer from the Mg atoms to the O ones takes place. As result, the O atoms obtain major negative charge (mean valence −1.77) while the Mg ones gain a bigger positive charge (mean valence +1.76) as compared with the bulk case (mean valence value −1.41 for O and +1.49 for Mg). This charge increase mechanism at the MgONW produces a bigger attraction between Mg and O atoms along the z direction in the 1D structure, which explains the observed contraction. Similar results are observed in the nanostructures containing magnetite. This aforementioned contraction along z increases from the MNW to the CSNT, and finally it presents its biggest value for the MNT, the hollow structure, with a major free external and internal surface area.

Figures 2 and 3 show the radial distribution functions for all the samples. For comparison, bulk Fe_3O_4 has been included in both figures. The first general observation is related to the fact that the nanostructures present ranges for the bond distances (distance distribution), centered in the bond equilibrium distances occurring for the bulk cases. Also, in general, a contraction of the nn distances is obtained at the surface, while dilated bonds can be observed at the internal part of the structures.

For example, while in bulk Fe_3O_4 the nn distance for bonds Fe_A-O is 1.90 Å, in the CSNT, MNW, and MNT these bonds adopt distances as small as 1.80, 1.78, and 1.73 Å, respectively. This corresponds to percentages of contraction of 5.3%, 6.3%, and 8.9% for the Fe_A-O bonds in the respective systems.

We confirmed that these changes take place predominantly at the surfaces, and they can be understood as a consequence of a decrease in the charge of the Fe atoms (i.e., an increase in the valence) as due to the symmetry breaking and reduced coordination. In contrast, at the interior of the structures, in general, Fe atoms exhibit an increased charge (valence reduced) as compared with the nominal values of the bulk

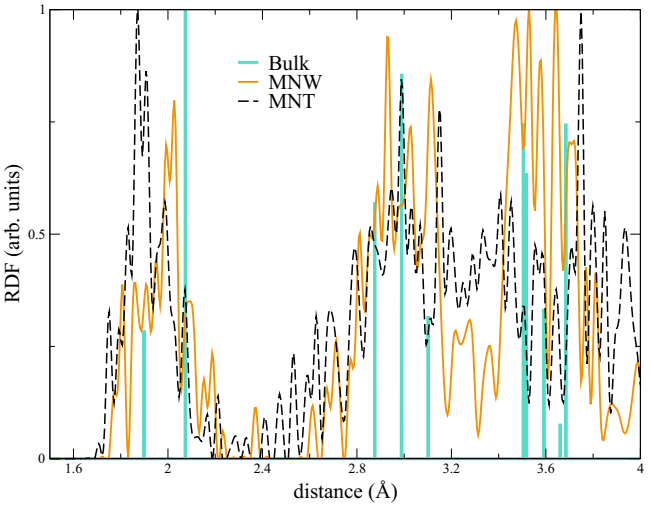

FIG. 2. (Color online) RDF for bulk Fe_3O_4 (cyan vertical bars), MNW (orange continuous), and MNT (black dashed). The cyan vertical bars mark, from the left to the right, the following distances (in Å) for bonds in bulk Fe_3O_4: Fe_A-O (1.90), Fe_B-O (2.08), O-O (2.88), Fe_B-Fe_B and O-O second nn (2.99), O-O third nn (3.10), Fe_A-Fe_B (3.51), Fe_A-O second nn (3.52), Fe_B-O second nn (3.59), Fe_A-Fe_A (3.66), and Fe_B-O third nn (3.69).

case, and distances are closer to the bulk values. MNT is the structure with larger surface (external and internal), and the one which presents a bigger contraction of the nn bonds (see Table IV).

The RDFs reported in Figs. 2 and 3 show also maxima distances for the nn bonds. For instance, in the MgONW case, the values 2.17, 3.01, and 3.10 Å hold for the bonds Mg-O, Mg-Mg, and O-O, respectively. For the MNW we found 2.01 and 2.38 Å for the Fe_A-O and Fe_B-O bonds, and 2.00 and 2.31 Å for the Fe_A-O and Fe_B-O bonds, in the MNT case.

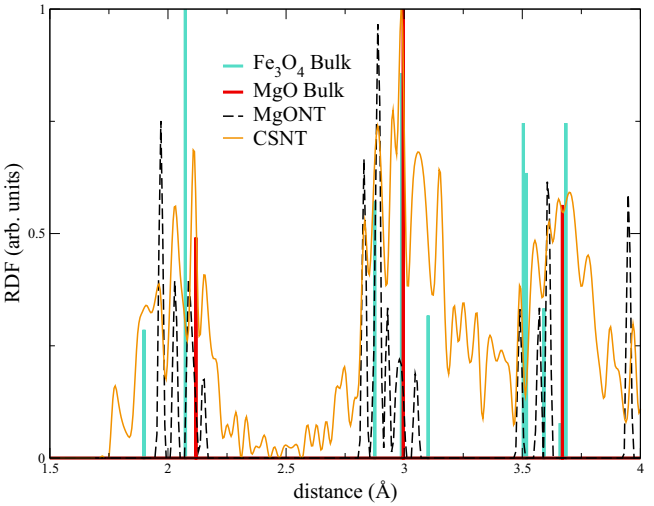

FIG. 3. (Color online) RDF for bulk Fe_3O_4 (cyan vertical bars), bulk MgO (red vertical bars), MgONT (black dashed), and CSNT (orange continuous). The red vertical bars mark, from the left to the right, the following distances (in Å) for bonds in bulk MgO: Mg-O (2.12), Mg-Mg (3.00), O-O (3.00), and Mg-O second nn (3.67).

TABLE IV. Minimum distances (in Å) and contraction percentages (within parentheses), taking the bulk value as reference, for the different types of bonds in the relaxed 1D nanostructures.

Bond type	MgONW	MNW	MNT	CSNT
Fe_A-O		1.78 (6.3)	1.75 (7.9)	1.80 (5.3)
Fe_B-O		1.81 (13.0)	1.73 (16.8)	1.81 (13.0)
Fe_B-Fe_B		2.65 (11.4)	2.72 (9.0)	2.56 (14.4)
Fe_A-Fe_B		2.94 (16.2)	2.72 (22.5)	2.73 (22.2)
Fe_A-Fe_A		3.36 (8.2)	2.69 (26.5)	2.42 (33.9)
O-O	2.90 (0.7)	2.62 (9.0)	2.36 (18.0)	2.63 (8.7)
Mg-O	1.99 (6.1)			2.02 (4.7)
Mg-Mg	2.85 (5.0)			2.80 (6.7)

Another general observation is that the tetrahedral and octahedral environments for Fe atoms appear with some distortion in MNW and CSNT. Bigger distortions for these substructures are observed in the MNT, due to the larger surface present on it.

Despite these distortions and all the reported changes in the atomic distances (due to the presence of the mentioned surfaces), an interesting observation should be highlighted concerning the type of bonding occurring between the atoms of each sample: whenever the MNT and the MgONW are brought together to compose the CSNT, the character of the bonds remains as in the original subsystems; i.e., at the core, the MgO bonds keep their ionic character, while at the shell (Fe_3O_4) a charge distribution is observed in between atoms and a covalent character is revealed in the bonds. This can be observed in Fig. 4 where different views of the charge density for the CSNT are presented.

B. Electronic properties

Regarding the electronic properties, we have computed the electronic density of states (DOS) of the relaxed bulk MgO and bulk magnetite, for comparison purposes. All energies are relative to the Fermi level. Figure 5 shows the total electronic DOS for bulk MgO and MgONW. As expected, no polarization was found either for the bulk case or for the MgONW. The DOSs in both cases are composed by a deep O 2*s* band separated from the occupied bands by a gap of around 11 eV. These states are formed mainly by O 2*p* states plus a very small contribution of Mg states, indicating the ionic character of the bonds between Mg and O atoms. The conduction band is composed by O 2*p* antibonding states plus a contribution of the Mg atoms as well.

The bulk MgO is an insulator with an electronic band gap around 4.6 eV. Due to the well known underestimation of the band gap by DFT-GGA band structure calculations [65,66], this value is less than the experimental result. However, a fair agreement is obtained when compared with other first-principles reports [60,61]. Despite its inaccuracy, it offers, qualitatively, a reasonable description of such systems. For the MgONW the band gap drops to 3.1 eV, in agreement with other first-principles studies on MgO nanotubes [38,60,61].

This reduction in the band gaps of the MgONW as compared with bulk MgO (32%) is mainly due to a decrease in the energy of the unoccupied O 2*p* states at the surface

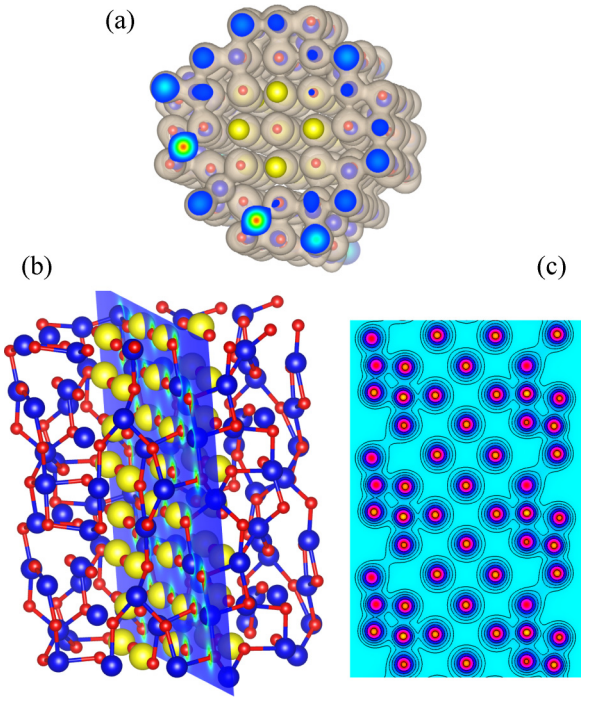

FIG. 4. (Color online) Charge density for the CSNT. (a) Top view; yellow spheres represent Mg atoms, while the blue and red ones stand for Fe and O, respectively. (b) Lateral view of the structure with a selected plane; color scheme for atoms remains as in (a). (c) Contour curves of the charge density on the plane indicated in (b); colors indicate different charge magnitudes.

atoms, which makes the conduction band move towards the Fermi level, and, consequently, the gap is smaller. This could be due to an effect of the system confinement, as will be discussed in more detail below. While the conduction band is largely flattened due to the confinement, the valence band has almost the same dispersion as the bulk. Therefore, it is

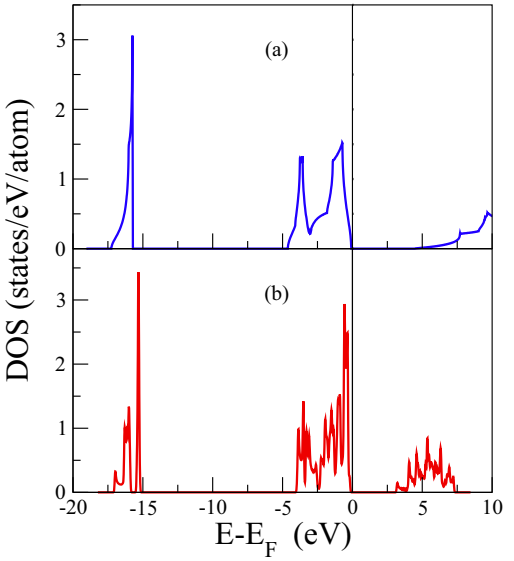

FIG. 5. (Color online) Total DOS for bulk MgO (a) and MgONW (b). Fermi level is located at zero energy.

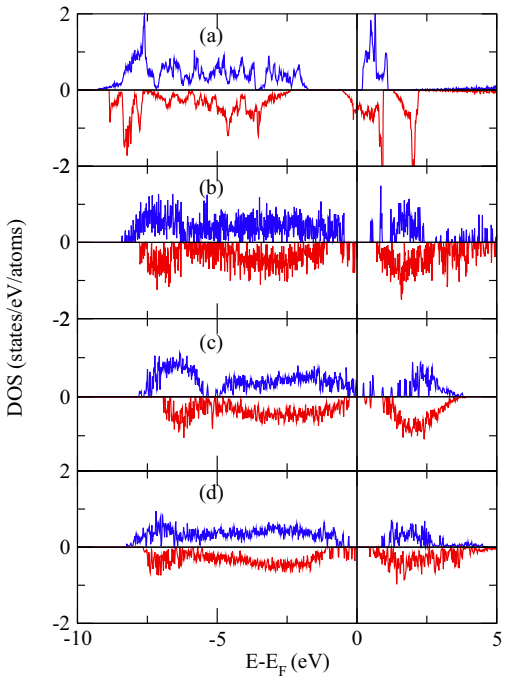

FIG. 6. (Color online) Total electronic DOS for bulk Fe_3O_4 (a), MNW (b), MNT (c), and CSNT (d). Fermi level is located at zero energy.

expected that hole conduction is not affected when compared with bulk, but it is modified due to the band gap reduction. In contraposition to the bulk case, for the MgONW the increase in the amount of peaks in the DOS is evident since, due to the confinement effect, structurally nonequivalent atoms split, giving rise to new electronic states. Bulk magnetite exhibits a half-metallic behavior ($\Delta_g = 0$) with the Fermi level located in the middle of the minority spin Fe_B band [Fig. 6(a)], in agreement with other reports [17,67,68]. From an analysis of the partial DOS computed by orbitals and atomic contributions (not shown), it is concluded that the Fe 3*d* orbitals have the major contributions in the valence and conduction bands.

In more detail, the energy spectra are formed by the low-lying quasicore O 2*s* states plus a very small contribution of the Fe 3*d* orbitals that are separated from the valence band by a wide gap (9.77 eV). This valence band is composed of Fe 3*d* plus O 2*p* orbitals. The conduction band [the minority spin channel in Fig. 6(a)] consists mainly of octahedral Fe 3*d* orbitals, while the majority spin conduction band is formed by tetrahedral Fe 3*d* states hybridized with O 2*p* orbitals. Differences in the contributions of *A* and *B* sites are consistent with the antiparallel alignment between *A* and *B* sublattices, in agreement with a ferrimagnetic state.

As we can see from Fig. 6, the DOS of the cylinder nanostructures barely resembles the bulk case: in all three Fe_3O_4 nanostructures [Figs. 6(b)–6(d)] the DOS is very spread on energy. However each electronic state has almost no dispersion (confirmed by inspection of the band structures, not shown here).

Figure 6(b) shows the total DOS for the MNW. As a first observation, differently from the half-metallic behavior observed in the bulk case, the MNW exhibits a semiconductor character with a gap of 0.471 eV taking place between the valence band in the minority spin channel and the conduction band at the majority spin channel; i.e., in this case the excitation of the electrons should occur through a spin inversion. The observed gaps for each spin channel are 0.931 eV (up) and 0.695 eV (down). The discrete character is ascribed to the presence of the free surface, which allows a certain degree of structural disorder and, in consequence, the apparition of many new states. The bands are displaced towards greater values of energy in comparison with the bulk case. Also a set of isolated subbands appears centered at around 0.5 eV (spin up), and between −0.6 eV and the Fermi level (spin down), which is the valence band for this structure.

From the orbital and atomic contributions to the partial DOS (not shown) we observe a very similar composition of the total DOS of the MNW as compared with the bulk magnetite; i.e., the deep bands consist mainly of O 2*s* states along with a small contribution of the Fe 3*d* orbitals. A subband arises at around −16.3 eV and a big gap of around 7.9 eV separates this minority subband from the valence band, which is also composed mainly of Fe 3*d* orbitals plus a small contribution of the O 2*p* orbitals. Also, the conduction band consists mainly of Fe 3*d* orbitals and a minor contribution of O 2*p* states. We observe that the valence band is composed of 3*d* orbitals coming from undercoordinated Fe atoms now present in this structure due to the free surface.

At this point, having in mind a potential application, it is relevant to highlight the mentioned n-p and p-n type carrier transitions [36]. In their work, Lee and colleagues experimentally studied the electronic properties of α-Fe_2O_3 nanowires and found that they exhibit p-type transport naturally and that, after an annealing process under reductive atmosphere, the p- to n-type transition takes place due to the conversion into magnetite nanowire [37]. Observation of the p-type nature of α-Fe_2O_3 nanowires, the n-type nature of MNWs, and the p-n and n-p transitions obtained through annealing processes between them allows us to think of promising technological applications of these magnetite-based nanostructures to nanoelectronics devices in the near future. In particular, our band structure analysis seems to indicate that magnetite nanowires have the possibility to be used in spin filtering due to the disparity between the spin character corresponding to the conduction when compared to the valence spin.

The total DOS for the MNT appears in Fig. 6(c). As the MNW, the MNT also exhibits a semiconductor character but with a minor value for the gap of 0.201 eV of the majority channel (0.564 eV for the minority spin channel). Differently from the MNW case, here the electronic excitation can take place without an inversion of the spins and could have implications in spintronics, where selected spin channels have preference.

In general, the composition of the total DOS is similar to the bulk and MNW cases. Some differences can be noticed in the bands near the Fermi level. Now both the valence and conduction bands are composed of hybridized Fe 3*d* and O 2*p* states. Our results suggest that, due to the major degree of disorder in this structure (since in the MNT there is a greater number of surface atoms), the observed increase of the energy levels near the Fermi energy and the hybridization

process between Fe and O are the responsible facts for the decrease in the band gap as compared with the MNW system. Moreover, this hybridization has been also experimentally observed in related nanostructures through EELS and ELNES analysis [36].

In Fig. 6(d) we present the total DOS for the core/shell structure. In this case the magnetite is built around the MgO wire, as in the experimental situation [20,25,30], and the free surface diminishes as compared with the MNT case; i.e., now the free surface is due only to the external surface of the cylinder. The semiconductor character remains with a gap of 0.522 eV for the minority spin channel (and 1.203 eV for the majority spin channel). This band gap, greater than the one of the MNT, can be understood as result of the presence of no hybridized states in the valence band, as in the MNW system. No spin inversion is required in an electronic excitation and the spin conduction channel remains unaltered.

C. HOMO-LUMO analysis and magnetic properties

Figure 7 shows a sketch of the HOMO and LUMO for the MNW, MNT, and CSNT. As observed, the electronic states for these quasi-1D systems turned out to be localized around small clusters of atoms. Interestingly, the mechanism behind this strong and unexpected electronic localization is not the disorder, at least not directly; instead, it seems to be caused by the strong charge transfer taking place among some nearest neighbors (see previous discussion on Bader charge analysis). Further, despite the freestanding MgONT showing a DOS similar to the bulk case, and the projected band structure indicating extended electronic states, when embedded into the CSNT, the MgO electronic structure loses its extended character, becoming localized.

Therefore, we cannot take for granted that 1D Fe_3O_4-based nanostructures—in this case nanocylinders—will resemble the bulk properties of magnetite. Even more, in a core/shell structure, the embedded system can lose its own nature due to the interaction with the oxide (as the MgO this time). Interestingly, from the point of view of applications, the strong localization regime observed in these structures can be quite useful. In particular, the resistance will increase exponentially with the length of wire [69], which offers the exciting potential of, technologically, tailoring resistances through small changes in the length of the nanostructure. Moreover, since no overlap between HOMO and LUMO is observed, increased magnetoresistance applications can be inferred for these nanotubes.

Concerning the degree of spin polarization (SP), since transport is related to states around the Fermi energy, we preferred to define a small range of energy instead of applying the usual definition of this quantity (computed just at the Fermi energy and often applied to ferromagnets) [70]. In our case we have taken $[-0.5,0]$ eV as the mentioned range of energies and the results indicate that the SP is smaller for the CSNT case than for the MNW and MNT structures. In any case, we should point that even though there is a particular tendency to increase the spin polarization in MNW and MNT as compared with CSNT, it is reduced by the important surface reconstruction in these 1D systems as compared with the bulk case. It is worth highlighting that an inversion of the majority/minority spin takes place in the MNT case as compared with the MNW and CSNT in the transport scheme, as has been previously mentioned. In any case, the fact that polarization is changed by a change in dimensionality should affect the magnetoresistivity of the sample. These last facts project venues for potential technological applications in the field of nanoelectronics.

From the band structure for the MgONW system (not shown), notable differences are obtained as compared with the bulk case; the dispersion of the band in the MgONW is smaller than in the bulk, suggesting a smaller interaction between adjacent cells along the z direction. The band structure (not shown) confirms the half-metallic feature of bulk magnetite since the spin-down electrons tend to intersect the Fermi level. This fact is in agreement with some other DFT results reported

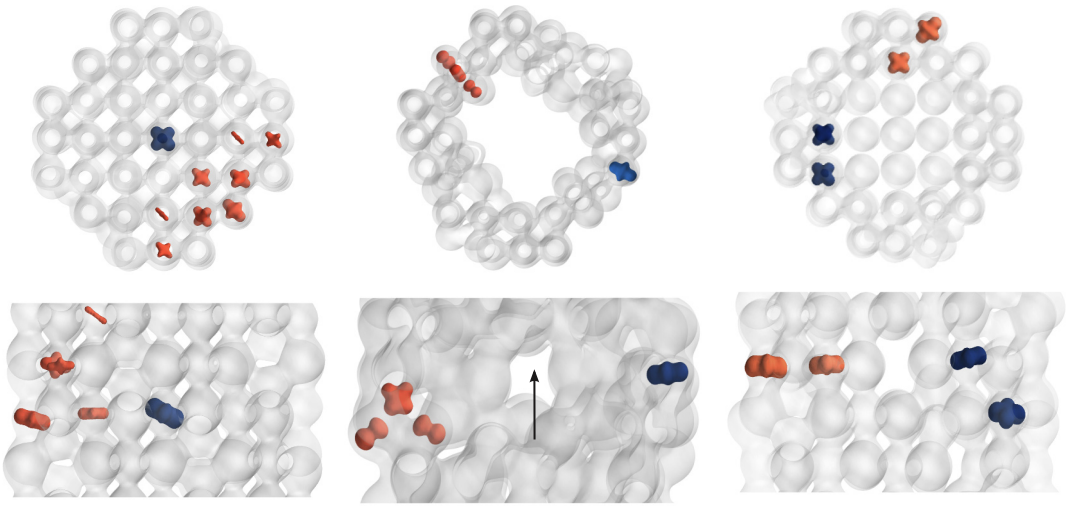

(a) MNW (b) MNT (c) CSNT

FIG. 7. (Color online) Localization of the HOMO (red-gray) and LUMO (blue-dark gray) on real space around a small cluster (molecular-like bonding), indicating a strong localization regime. The arrow points to the tube axis, and the gray spheres are the total charge density. The isovalues are computed at 0.2 eV/Å^3.

by Friák *et al.* [68]. From the other side, since the energetic scheme of the quasi-1D systems is predominantly dominated by *d* orbitals, as discussed previously, their band structures (not shown) appear almost dispersionless. Through the analysis of the effective mass around the Γ point, we observe that the MNT offers larger mobility for the electrons than the MNW. Once the MgO occupies the internal space inside the MNT to form the CSNT, a similar value for the effective mass is obtained as compared with the MNT case. This indicates that the mobility of electrons is not appreciably affected by the presence of this insulator material.

On the other side, magnetic properties from Table III indicate that neither the bulk MgO nor the MgONW present magnetic behavior, as expected. Thus, the magnetism in the rest of the structures is indebted to the Fe atoms coming from magnetite. A sensitive increase in the magnetization per Fe atom is observed in the 1D structures as compared with bulk magnetite. This increment of magnetic moment goes from the CSNT, passing by the MNT, to the MNW in increasing order with percentages from 14%, 25%, up to 33%, respectively. Again, this is related to the orbital character responsible for the atomic magnetic moment but it is also related to less atomic overlap, which then decreases the energy dispersion.

D. Mechanical properties

To evaluate the effect of deformation on the properties, the considered one-dimensional structures have been submitted to stress and compression along the *z* direction. Figure 8 shows the energy as function of the percentage of strain. Adequate functions have been employed to fit the behavior around the equilibrium points. The elastic constants can be computed from these results, giving the values 475.5, 186.7, 241.7, and 2464.7 N/m for MgONW, MNW, MNT, and CSNT, respectively.

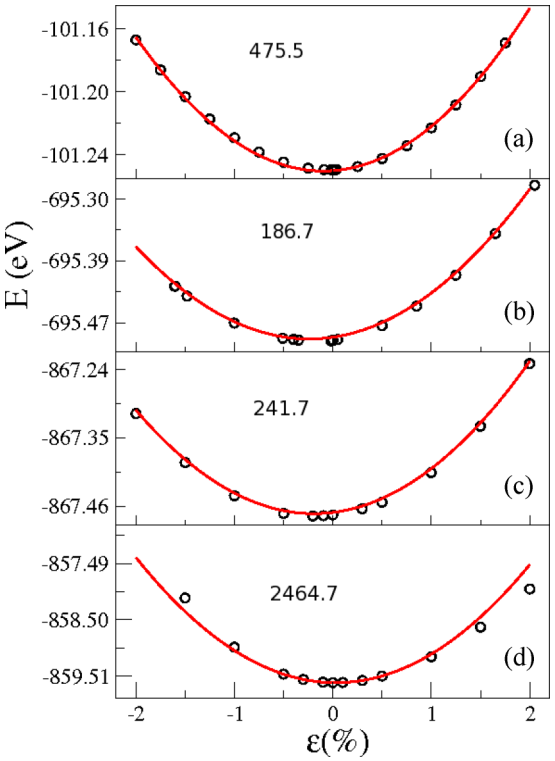

FIG. 8. (Color online) Energy as function of strain (ϵ) for MgONW (a), MNW (b), MNT (c), and CSNT (d). Inside each case we report the resultant value for the elastic constant in N/m.

As observed, the MNT structure presents a bigger value for the elastic constant as compared with the MNW. This result can be explained through the presence of major internal and external surface, which generates a major interaction between the atoms in the MNT due to the spread behavior of the charge distribution along the *z* direction, as discussed previously. Notably, a higher value (one order of magnitude superior) is obtained for the combined core-shell structure as compared with its isolated components (MgONW and MNT). It shows the harder character of this CSNT as result of the superposed effect of its individual parts.

Very small changes can be obtained for the MgONW whenever it is compressed or elongated at about 10% as compared with the free MgONW. As a general observation, the DOS keeps its general structure as the nondeformed case. Table V shows the dispersion for the two former bands upside (denoted b1 and b2) and downside (b-1 and b-2) the Fermi level for MgONW, MNT, and CSNT. As observed, in the MgONW case the major effect is obtained when a contraction is applied, specially in the b-1 band, which presents a variation of 156%, differently from the stressed case, where the dispersion change reaches a 40% as compared with the nanowire in equilibrium.

In the case of MNT the variations reach 2% with respect to the pristine MNT, which corresponds to a pressure of 0.1 GPa applied along the *z* direction. From the DOS in these cases a slight reduction in the gap is observed. However the contribution scheme of the partial DOS remains very similar to the unstressed tube.

The values of stress and contraction for the supercell of CSNT go from 8.66 to 8.16 Å, which corresponds to a 3% of

TABLE V. Band dispersion for MgONW (under 10% strain), MNT (under 2% strain) and CSNT (under 3% strain). Data are reported for the two former bands upside the Fermi level (b1 and b2) and the two former ones downside it (b-1 and b-2). Inside the parentheses we report the percentage of deviation with respect to the equilibrium values of dispersion, reported in the first column.

	Equilibrium	Contraction (% diff.)	Stress (% diff.)
MgONW			
b1	2.297	2.882 (25.5)	1.986 (14)
b2	1.675	1.995 (19)	1.349 (20)
b-1	0.149	0.381 (156)	0.09 (40)
b-2	0.091	0.134 (47)	0.09 (1)
MNT			
b1	0.1	0.004 (96)	0.016 (84)
b2	0.001	0.007 (600)	0.008 (700)
b-1	0.02	0.008 (60)	0.004 (80)
b-2	0.024	0.024 (0)	0.015 (37.5)
CSNT			
b1	0.19	0.006 (97)	0.003 (98)
b2	0.031	0.01 (68)	0.001 (98)
b-1	0.002	0.022 (1000)	0.01 (400)
b-2	0.009	0.027 (200)	0.024 (177)

variation respect to the nonaffected core-shell structure (whose equilibrium value is 8.41 Å). The DOS shows a very similar behavior as compared with the equilibrium case, even though the band gap for the spin-up channel is slightly wider under stress and slightly shorter under compression.

These results provide a solid base for future research in applied fields such as magnetoelectromechanical effects.

IV. CONCLUSIONS

Different magnetite-based quasi-1D nanostructures have been considered in this study including nanowires (MNW), nanotubes (MNT), and MgO/Fe_3O_4 core/shell nanotubes (CSNT). For comparison purposes we have considered bulk magnetite, MgO nanowires, and MgO bulk samples. The interest in MgO arises originally since, due to its small cell mismatch with magnetite, it is used as template element for the construction of the core/shell structures [20,24,25,30]. The structural, electronic, and magnetic properties of the mentioned quasi-1D structures were evaluated. CSNT obtains a configuration with favorable cohesive energy per atom as compared with MgONW and MNT (the two structures that compose the CSNT), and MNW is the most stable system. These quasi-1D systems have been found of potential interest for several discussed applications. In particular, due to its properties, MNT and MNW can be useful in transport developments such as spin filtering. Also, regarding the biocompatibility of magnetite, the MNTs can be considered as a very promising material for the development of the nanosyringe application [32,33], whereas the CSNT system could be used in applications related to magnetoresistance effects [20,24,25,30,69]. Finally, the effect of stress on the properties has been tested by submitting the quasi-1D structures to deformations along the z direction, and the elastic constants have been computed and reported with the aim to provide a useful base for future research in applied fields.

ACKNOWLEDGMENTS

The authors are grateful for support from several projects: IN10221CE and IN10197CE CODI-SUI projects of the GICM and GES Groups at Universidad de Antioquia (UdeA); FONDECYT Grants No. 1100365 and No. 11110510; Millennium Science Nucleus "Basic and Applied Magnetism" P10-061-F; Financiamiento basal para centros científicos y tecnológicos de excelencia FB 0807; and the Marie Curie Actions from the European Union in the international incoming fellowships (Grant No. PIIFR-GA-2011-911070) and the Donors of the American Chemical Society Petroleum Research Fund for partial support of this research under Contract No. 54075-ND10. J.M.-Z. thanks Universidad de Antioquia for a "Dedicación Exclusiva" program (2013-2014). We also acknowledge the computer time provided by TACC, University of Texas Supercomputer Center, as well as CNS, IPICYT, México and Super Computing System (Mountaineer) at WVU, which are funded in part by the National Science Foundation EPSCoR Research Infrastructure Improvement Cooperative Agreement 1003907, the state of West Virginia (WVEPSCoR via the Higher Education Policy Commission) and WVU.

[1] H. J. Fan, U. Gösele, and M. Zacharias, Small **3**, 1660 (2007).
[2] E. Arisi, I. Bergenti, M. Cavallini, M. Murgia, A. Riminucci, G. Ruani, and V. Dediu, J. Magn. Magn. Mater. **316**, 410 (2007).
[3] M. Klokkenburg, B. H. Erné, J. D. Meeldijk, A. Wiedenmann, A. V. Petukhov, R. P. A. Dullens, and A. P. Philipse, Phys. Rev. Lett. **97**, 185702 (2006).
[4] W. Schnelle, A. Leithe-Jasper, M. Schmidt, H. Rosner, H. Borrmann, U. Burkhardt, J. A. Mydosh, and Y. Grin, Phys. Rev. B **72**, 020402 (2005).
[5] M. Zahn, J. Nanopart. Res. **3**, 73 (2001).
[6] Y. C. Sui, R. Skomski, K. D. Sorge, and D. J. Sellmyer, J. Appl. Phys. **95**, 7151 (2004).
[7] S. O. Hwang, C. H. Kim, Y. Myung, S.-H. Park, J. Park, J. Kim, C.-S. Han, and J.-Y. Kim, J. Phys. Chem. C **112**, 13911 (2008).
[8] D. Lee, R. E. Cohen, and M. F. Rubner, Langmuir **23**, 123 (2007).
[9] H.-M. Fan, J.-B. Yi, Y. Yang, K.-W. Kho, H.-R. Tan, Z.-X. Shen, J. Ding, X.-W. Sun, M. C. Olivo, and Y.-P. Feng, ACS Nano **3**, 2798 (2009).
[10] C. A. Haberzettl, Nanotechnology **13**, R9 (2002).
[11] A. K. Gupta and M. Gupta, Biomaterials **26**, 3995 (2005).
[12] A. H. Latham and M. E. Williams, Acc. Chem. Res. **41**, 411 (2008).
[13] M. Ferrari, Nat. Rev. Cancer. **5**, 161 (2005).
[14] S. J. Son, J. Reichel, B. He, M. Schuchman, and S. B. Lee, J. Am. Chem. Soc. **127**, 7316 (2005).
[15] D. Kim, S. Lee, K. Im, K. Kim, K. Kim, I. Shim, M. Lee, and Y.-K. Lee, Current Appl. Phys. **6**, e242 (2006).
[16] J.-H. Park, G. von Maltzahn, L. Zhang, M. P. Schwartz, E. Ruoslahti, S. N. Bhatia, and M. J. Sailor, Adv. Mater. **20**, 1630 (2008).
[17] S. López, A. H. Romero, J. Mejía-López, J. Mazo-Zuluaga, and J. Restrepo, Phys. Rev. B **80**, 085107 (2009).
[18] X. Wen, S. Wang, Y. Ding, Z. L. Wang, and S. Yang, J. Phys. Chem. B **109**, 215 (2005).
[19] J. R. Morber, Y. Ding, M. S. Haluska, Y. Li, J. P. Liu, Z. L. Wang, and R. L. Snyder, J. Phys. Chem. B **110**, 21672 (2006).
[20] Z. Liu, D. Zhang, S. Han, C. Li, B. Lei, W. Lu, J. Fang, and C. Zhou, J. Am. Chem. Soc. **127**, 6 (2005).
[21] J. Chen, L. Xu, W. Li, and X. Gou, Adv. Mater. **17**, 582 (2005).
[22] J. Liu, Y. Li, H. Fan, Z. Zhu, J. Jiang, R. Ding, Y. Hu, and X. Huang, Chem. Mater. **22**, 212 (2010).
[23] K. Pitzschel, J. M. M. Moreno, J. Escrig, O. Albrecht, K. Nielsch, and J. Bachmann, ACS Nano **3**, 3463 (2009).
[24] Z.-M. Liao, Y.-D. Li, J. Xu, J.-M. Zhang, K. Xia, and D.-P. Yu, Nano Letters **6**, 1087 (2006).
[25] D. Zhang, Z. Liu, S. Han, C. Li, B. Lei, M. P. Stewart, J. M. Tour, and C. Zhou, Nano Lett. **4**, 2151 (2004).
[26] M. Abid, J.-P. Abid, S. Jannin, S. Serrano-Guisan, I. Palaci, and J.-P. Ansermet, J. Phys.: Condens. Matter **18**, 6085 (2006).
[27] Y.-J. Chen, F. Zhang, G.-g. Zhao, X.-y. Fang, H.-B. Jin, P. Gao, C.-L. Zhu, M.-S. Cao, and G. Xiao, J. Phys. Chem. C **114**, 9239 (2010).
[28] C.-L. Zhu, M.-L. Zhang, Y.-J. Qiao, G. Xiao, F. Zhang, and Y.-J. Chen, J. Phys. Chem. C **114**, 16229 (2010).

[29] H. Fan, M. Knez, R. Scholz, K. Nielsch, E. Pippel, D. Hesse, U. Gösele, and M. Zacharias, Nanotechnology **17**, 5157 (2006).
[30] S. Han, C. Li, Z. Liu, B. Lei, D. Zhang, W. Jin, X. Liu, T. Tang, and C. Zhou, Nano Lett. **4**, 1241 (2004).
[31] S. R. Chun, W. A. Sasangka, M. Z. Ng, Q. Liu, A. Du, J. Zhu, C. M. Ng, Z. Q. Liu, S. Y. Chiam, and C. L. Gan, Small **9**, 2545 (2013).
[32] T. A. Hilder and J. M. Hill, Small **5**, 300 (2009).
[33] T. A. Hilder and J. M. Hill, J. Comput. Theor. Nanosci. **5**, 2153 (2008).
[34] G. Korotcenkov, V. Brinzari, V. Golovanov, A. Cerneavschi, V. Matolin, and A. Tadd, Appl. Surf. Sci. **227**, 122 (2004).
[35] A. Gurlo, N. Brsan, A. Oprea, M. Sahm, T. Sahm, and U. Weimar, Appl. Phys. Lett. **85**, 2280 (2004).
[36] Y.-C. Lee, Y.-L. Chueh, C.-H. Hsieh, M.-T. Chang, L.-J. Chou, Z. L. Wang, Y.-W. Lan, C.-D. Chen, H. Kurata, and S. Isoda, Small **3**, 1356 (2007).
[37] Y.-L. Chueh, M.-W. Lai, J.-Q. Liang, L.-J. Chou, and Z. Wang, Adv. Funct. Mater. **16**, 2243 (2006).
[38] I. R. Shein, A. N. Enyashin, and A. L. Ivanovskii, Phys. Rev. B **75**, 245404 (2007).
[39] P. Hohenberg and W. Kohn, Phys. Rev. **136**, B864 (1964).
[40] W. Kohn and L. J. Sham, Phys. Rev. **140**, A1133 (1965).
[41] G. Kresse and J. Furthmüller, Comput. Mater. Sci. **6**, 15 (1996).
[42] G. Kresse and J. Furthmüller, Phys. Rev. B **54**, 11169 (1996).
[43] P. E. Blöchl, Phys. Rev. B **50**, 17953 (1994).
[44] G. Kresse and D. Joubert, Phys. Rev. B **59**, 1758 (1999).
[45] J. P. Perdew, K. Burke, and M. Ernzerhof, Phys. Rev. Lett. **77**, 3865 (1996).
[46] S. L. Dudarev, G. A. Botton, S. Y. Savrasov, C. J. Humphreys, and A. P. Sutton, Phys. Rev. B **57**, 1505 (1998).
[47] H.-T. Jeng, G. Y. Guo, and D. J. Huang, Phys. Rev. B **74**, 195115 (2006).
[48] V. I. Anisimov, I. S. Elfimov, N. Hamada, and K. Terakura, Phys. Rev. B **54**, 4387 (1996).
[49] V. N. Antonov, B. N. Harmon, and A. N. Yaresko, Phys. Rev. B **67**, 024417 (2003).
[50] V. I. Anisimov, J. Zaanen, and O. K. Andersen, Phys. Rev. B **44**, 943 (1991).
[51] Z. Łodziana, Phys. Rev. Lett. **99**, 206402 (2007).
[52] F. Birch, Phys. Rev. **71**, 809 (1947).
[53] G. Henkelman, A. Arnaldsson, and H. Jónsson, Comput. Mater. Sci. **36**, 354 (2006).
[54] P. Piekarz, K. Parlinski, and A. M. Oleś, Phys. Rev. Lett. **97**, 156402 (2006).
[55] P. Piekarz, K. Parlinski, and A. M. Oleś, Phys. Rev. B **76**, 165124 (2007).
[56] J. P. Wright, J. P. Attfield, and P. G. Radaelli, Phys. Rev. B **66**, 214422 (2002).
[57] J. P. Wright, J. P. Attfield, and P. G. Radaelli, Phys. Rev. Lett. **87**, 266401 (2001).
[58] R. Aragón, Phys. Rev. B **46**, 5328 (1992).
[59] C. Haavik, S. Stølen, H. Fjellvåg, M. Hanfland, and D. Häusermann, Am. Mineral. **85**, 514 (2000).
[60] A. N. Enyashin, I. R. Shein, and A. L. Ivanovskii, Phys. Rev. B **75**, 193408 (2007).
[61] P. K. de Boer and R. A. de Groot, J. Phys.: Condens. Matter **10**, 10241 (1998).
[62] D. M. Roessler and W. C. Walker, Phys. Rev. **159**, 733 (1967).
[63] A. Gueddim, N. Bouarissa, and A. Villesuzanne, Phys. Scrip. **80**, 055702 (2009).
[64] Y. Fei, Am. Mineral. **84**, 272 (1999).
[65] J. Robertson, K. Xiong, and S. Clark, Thin Solid Films **496**, 1 (2006).
[66] L. J. Sham and M. Schlüter, Phys. Rev. Lett. **51**, 1888 (1983).
[67] Z. Zhang and S. Satpathy, Phys. Rev. B **44**, 13319 (1991).
[68] M. Frik, A. Schindlmayr, and M. Scheffler, New J. Phys. **9**, 5 (2007).
[69] C. Gómez-Navarro, P. J. D. Pablo, J. Gómez-Herrero, B. Biel, F. J. Garcia-Vidal, A. Rubio, and F. Flores, Nat. Mater. **4**, 534 (2005).
[70] I. I. Mazin, Phys. Rev. Lett. **83**, 1427 (1999).